Int. J. Heat Mass Transfer. Vol. 31, No. 4, pp. 831–841, 1988
Printed in Great Britain

0017–9310/88 $3.00+0.00

Laminar free convection flow rate in a vertical tube

TETSU FUJII, SHIGERU KOYAMA and N. S. BUENCONSEJO, JR.
Institute of Advanced Material Study, Kyushu University, Kasuga-shi, Fukuoka 816, Japan

(*Received* 12 *December* 1986 *and in final form* 16 *September* 1987)

Abstract—This paper considers the flow rate of a laminar free convection inside a fully heated or a partly heated and partly cooled vertical tube placed in a large space. A theory based on a one-dimensional model which uses the Graetz solution for forced convection in a tube and which considers the pressure losses at the tube inlet and exit and in the hydrodynamic developing region is proposed for the range $Gr\,Pr < 100$. For the fully heated tube, the theory is compared with a two-dimensional numerical analysis and actual measurements using a quartz fiber anemometer. Their agreement is good when proper values of pressure loss coefficients are used in the theory. For the partly heated and partly cooled or partly adiabatic tube in thermally stratified and non-stratified ambients, the agreement between the theory and the experiment is also good. The effects of the tube-to-ambient temperature difference, the representative temperature of the stratified ambient, the tube length-to-diameter ratio and the temperature dependence of fluid properties upon the average mass velocity inside the tube are also clarified.

INTRODUCTION

IN 1866 Franz Grashof [1] presented a theory on draft generation through a chimney. In this theory a one-dimensional momentum equation containing the buoyancy term is solved by considering the variation of gas temperature, which is obtained by combining the energy equation and heat transfer through the duct wall. A numerical example of the theory for determining the height of a chimney for a boiler furnace using measured and assumed values for flow resistance through the gas passage is shown. This seems to be the first comprehensive work on free convection inside a vertical duct. Recently, numerous theoretical and experimental studies [2–32] concerning free convection in a vertical duct or parallel plates using two-dimensional momentum and energy equations are available. However, their main concerns are restricted to heat transfer characteristics and only Currie and Newman [11] and Aung *et al.* [18] measured the velocity distribution over the flow cross section although the prediction of the naturally convected mass flow rate is important to ventilation applications. Also, no study on the effect of ambient thermal stratification on free convection through a vertical tube has been carried out, except for the theoretical analysis by Lauber and Welch [9].

This paper aims to provide a simple and accurate method for predicting the free convection flow rate inside a vertical tube and to verify the method by comparing it with a two-dimensional numerical analysis and actual measurements.

SIMPLIFIED ONE-DIMENSIONAL THEORY

We consider the situation as follows: a vertical tube of inner diameter D and length L is placed in a fluid of temperature T_∞, the temperature of the inner surface of the tube is kept at T_w, and a resulting buoyancy driven flow occurs inside the tube. The present problem is to predict, with reasonable accuracy, the average mass velocity inside the tube by using a simple one-dimensional model.

To introduce the one-dimensional model, the following assumptions are made.

(1) The effect of buoyancy on the velocity profile within the tube cross section can be neglected; and the profile is hydrodynamically developed from the tube inlet or the same as that of Poiseuille flow.

(2) The effect of buoyancy on the temperature profile within the tube cross section can also be neglected; and the temperature profile is given by the Graetz solution for forced convection heat transfer.

(3) Temperature T, pressure p, velocity U and mass velocity G in the tube are values averaged over the cross-sectional area and density ρ and viscosity μ of the fluid are evaluated at T.

By integrating the conservation equations of mass and momentum within the cross-sectional area and by introducing the above assumptions, the following equations are derived:

$$G = \rho U = \text{const.} \tag{1}$$

$$\frac{4}{3}G^2\frac{\mathrm{d}}{\mathrm{d}x}\left(\frac{1}{\rho}\right) = -\frac{\mathrm{d}p^*}{\mathrm{d}x} + (\rho_\infty - \rho)g - \frac{32\mu G}{\rho D^2} \tag{2}$$

where x is the distance measured from the tube inlet in the direction of flow and g is the gravitational acceleration. The term on the left-hand side (inertia term) and the third term on the right-hand side (friction term) of equation (2) are derived by assumption (1). The first and the second terms on the right-hand side are derived by introducing

NOMENCLATURE

B	total buoyancy force, equation (9)
d	fiber diameter
D	inner diameter of tube
F	total wall frictional force, equation (8)
g	gravitational acceleration
G	average mass velocity, equation (1)
G_{exp}	measured average mass velocity
Gr	Grashof number, $g(T_w-T_0)r_w^4/(T_\infty v^2 L)$
G_{th}	theoretically predicted average mass velocity
k	thermal conductivity
k_1	coefficient, equation (15)
k_2	coefficient, equation (16)
k_3, k_4	coefficients, equation (17)
K_n	coefficient, equation (10), Appendix
l	fiber length
L	tube length
L^*	dimensionless tube length, $1/Gr$
L_h, L_u	heated, unheated tube lengths
L_1, L_2, L_3	lengths shown in Fig. 11
Nu	Nusselt number, $(\alpha r_w)/k$
p	static pressure
p^*	pressure defect, equation (3), $p-p_\infty$
Pr	Prandtl number
r	radial coordinate
r^*	dimensionless radial coordinate, Appendix, r/r_w
r_w	tube radius
Re	Reynolds number, GD/μ
T	temperature, and cross-sectional-area-averaged fluid temperature
T_c	temperature at tube center-line
T_w	wall temperature
T_∞	ambient temperature
$T_{\infty e}$	representative ambient temperature
u	local axial velocity in the tube
U	average axial velocity in the tube
w	volume flow rate, $2\pi\int_0^{r_w} ur\,dr = (G\pi r_w^2)/\rho$
W	dimensionless volume flow rate, $w/(\pi L\nu\, Gr)$
x	axial coordinate measured from the tube inlet in the direction of flow
x^+	dimensionless axial coordinate, equations (10) and (11), $(2x/D)(1/Re\,Pr)$.

Greek symbols

α	average heat transfer coefficient for the entire tube length, based on (T_w-T_0)
δ	deflection of quartz fiber
ζ_L	pressure loss coefficient due to flow expansion at tube exit
ζ_0	pressure loss coefficient due to flow contraction at tube entrance
θ_L	dimensionless cross-sectional area average fluid temperature at the tube exit, $(T_L-T_0)/(T_w-T_0)$
λ_n	nth eigenvalue, equation (10), Appendix
μ	dynamic viscosity
ν	kinematic viscosity
ξ	pressure loss coefficient for entrance developing region
ρ	density
ρ_m	parameter defined by equation (7).

Subscripts

c	at center-line of tube
D	lower tube
L	at tube exit
U	upper tube
w	at tube wall
x	at x
0	at tube inlet
∞	ambient.

$$p^* = p - p_\infty \tag{3}$$

where p is the static pressure inside the tube and p_∞ the static pressure of the ambient fluid at the same elevation.

We supplement the simplistic assumption (1) by considering the pressure losses due to velocity development in the entrance region and flow contraction at the tube inlet as shown in Fig. 1. The solid line represents the pressure in the developing region of an isothermal flow, and the dashed line represents the pressure corresponding to assumption (1). The maximum difference between these two lines is expressed by $\xi\rho U^2/2$, where the value of ξ varies with Reyn-

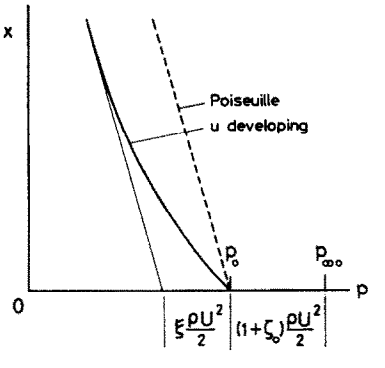

FIG. 1. Sketch of pressure distribution near the tube entrance.

olds number for low Reynolds number flows. The value given by Schmidt and Zeldin [33] is 1.4 for $Re = 100$ and that given by Chen [34] is 1.8 for $Re = 50$. The inlet static pressure p_0 is lower than the static pressure of the ambient fluid in the same elevation by $(1+\zeta_0)\rho_0 U_0^2/2$, where $\zeta_0\rho_0 U_0^2/2$ is caused by flow contraction near the tube inlet. The outlet static pressure p_L is lower than the static pressure of the ambient fluid in the same elevation by $(1-\zeta_L)\rho_L U_L^2/2$, where ζ_L is a factor to allow for incomplete recovery of pressure at the tube exit. Finally, the pressure defects at $x = 0$ and L are expressed as

$$p_0^* = -\tfrac{1}{2}(1+\zeta_0+\xi)\rho_0 U_0^2 \quad \text{at } x = 0 \tag{4}$$

$$p_L^* = -\tfrac{1}{2}(1-\zeta_L)\rho_L U_L^2 \quad \text{at } x = L \tag{5}$$

where the values of $\zeta_0 = 1$ and $\zeta_L = 0.4$ are given by Kays [35] in his experiment with isothermal flow conditions. Aihara and co-workers [20, 32], Quintiere and Mueller [21] and Dyer [23] employed $\zeta_0 = 0$ and $\zeta_L = 1$ in their theoretical analyses for a uniform inlet velocity profile.

Equation (2) is integrated from $x = 0$ to L subject to boundary conditions (4) and (5), and the following equation for mass velocity is derived by applying continuity equation (1)

$$G^2 + \rho_m F G - \rho_m B = 0 \tag{6}$$

where

$$\frac{1}{\rho_m} = \frac{5}{6}\left(\frac{1}{\rho_L} - \frac{1}{\rho_0}\right) + (\zeta_0+\xi)\frac{1}{2\rho_0} + \frac{\zeta_L}{2\rho_L} \tag{7}$$

$$F = \frac{32}{D^2}\int_0^L \left(\frac{\mu}{\rho}\right) dx \tag{8}$$

$$B = g\int_0^L (\rho_\infty - \rho)\, dx. \tag{9}$$

The axial temperature distribution T_x for the evaluation of ρ_m, F and B is available in accordance with assumption (2), as

$$\frac{T_x - T_w}{T_0 - T_w} = \sum_{n=1}^{\infty} K_n \exp(-\lambda_n^2 x^+) \tag{10}$$

$$x^+ = \frac{2x}{D\, Re\, Pr} \tag{11}$$

where the eigenvalues λ_n and coefficients K_n are given in the Appendix.

As the coefficients ρ_m, F and B are weak functions of G, equation (6) can be expressed as

$$G = \tfrac{1}{2}\rho_m F\left\{-1 + \left(1 + \frac{4B}{\rho_m F^2}\right)^{1/2}\right\} \tag{12a}$$

or

$$G = \frac{B}{F}\left\{1 - \frac{B}{\rho_m F^2} + \frac{2B^2}{\rho_m^2 F^4} - \cdots\right\}. \tag{12b}$$

Numerical calculations for obtaining the G value are carried out as follows. The tube length is divided into equally spaced sections of sizes $\Delta x = D/3$ near the entrance ($x^+ \leqslant 0.6$) and $\Delta x = 2/3D$ further downstream ($x^+ > 0.6$). Then, (i) we assume G and calculate T_x by equations (10) and (11) at every node, (ii) obtain μ and ρ corresponding to T_x, (iii) substitute ρ and μ into equations (8) and (9), and obtain F and B by Simpson's rule for integration and ρ_m using the assumed ξ, ζ_0 and ζ_L values, and (iv) obtain G by substituting ρ_m, F and B into equation (12a). Procedure (i)–(iv) is repeated until G converges.

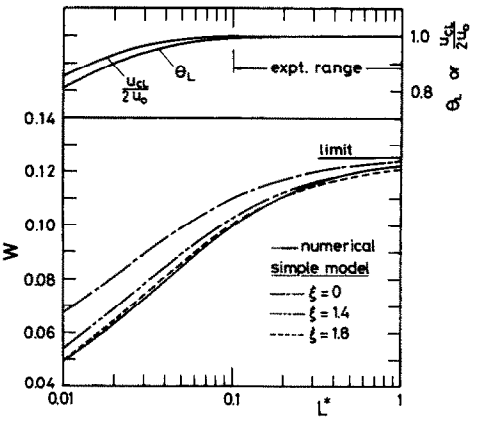

FIG. 2. Comparison between the volume flow rates predicted by the simplified model and the two-dimensional numerical analysis.

For long tubes ($L \gg D$) equation (12b) tends to

$$G = \frac{B}{F}. \tag{13}$$

COMPARISON BETWEEN THE SIMPLIFIED ONE-DIMENSIONAL MODEL AND THE TWO-DIMENSIONAL NUMERICAL ANALYSIS

The authors solved the usual two-dimensional boundary-layer-type mass, momentum and energy equations for free convection in a vertical tube by a finite difference method similar to that of Davis and Perona [14]. The pressure conditions at the inlet and exit were taken as $p_0^* = 0$ and $p_L^* = 0$. The fluid properties were assumed constant, except for the variation of density with temperature in the buoyancy term, and thus the volume flow rate w is constant throughout the tube length. This differs from the treatment of fluid properties in the simplified model, where fluid properties vary with temperature T and the average mass velocity G is constant throughout the tube length.

For comparing the simplified model with the results of the numerical analysis, the predicted G of the model is converted to dimensionless flow rate W by using values of ρ and μ at exit fluid temperature T_L. Further, the values of pressure coefficients in the model were taken as $\zeta_0 = -1$ and $\zeta_L = 1$ to conform with the tube-end conditions of the numerical analysis.

Figure 2 shows the variations of W with dimensionless tube length $L^* = 1/Gr$ as predicted by the simplified model and the two-dimensional numerical

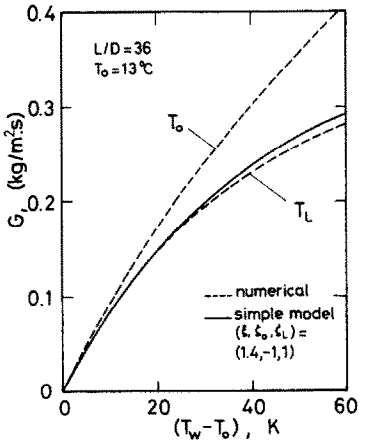

FIG. 3. Comparison between the average mass velocities predicted by the simplified model and the two-dimensional numerical analysis.

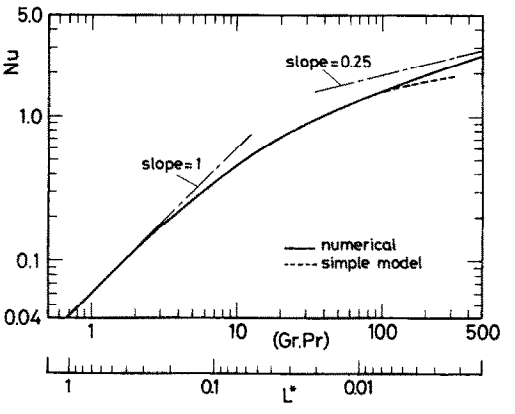

FIG. 4. *Nu* vs *Gr Pr* relationship predicted by the simplified model and the two-dimensional numerical analysis.

analysis. The curves for $\xi = 1.4$ and 1.8 of the model are closer to that of the numerical analysis, while the curve for $\xi = 0$, which neglects the entrance development loss, is considerably higher than that of the numerical analysis. The results for $\xi = 1.4$ and 1.8 also roughly demonstrate the dependence of ξ on *Re* for low Reynolds number flows, as in the present range where $L^* = 0.01$, 0.1 and 1 correspond to $Re = 50$, 100 and 120, respectively. All *W* predictions approach the limiting value of 1.25 as tube length increases or as *Gr* decreases. Also plotted in the figure are values of the cross-sectional area average temperature θ_L and the ratio of the center-line velocity to twice the inlet velocity $u_{cL}/2u_0$ at the tube exit. By comparing these curves with the *W* curves, it is recognized that the simplified model is also applicable to flows which remain hydrodynamically and thermally developing up to the tube exit.

Figure 3 shows comparison between the simplified model and the two-dimensional numerical analysis in terms of average mass velocity. The *W* values of the numerical analysis are converted to *G* with fluid properties based on fluid temperature T_0 at the tube inlet and T_L at the tube exit. The converted *G* values based on T_L are closer to those of the simplified model which means that the average temperature of the fluid within the tube is close to T_L. This illustrates the difficulty in applying the *W* results and the inappropriateness of the constant property assumption in the numerical analysis. Further, the difference between the *G* based on T_L and the model increases with $(T_w - T_0)$ which means that the difference increases as the length of the thermal entrance region increases.

Figure 4 shows the results for dimensionless heat transfer coefficient *Nu* of the numerical analysis and the simplified model. For $Gr\,Pr < 100$, the results of the model coincide with those of the numerical analysis. At low *Gr Pr* the flow becomes fully developed and the slope of the curve predicted by both solutions approaches 1. For large values of *Gr Pr* the slope of the curve predicted by the numerical analysis approaches the 1/4 power law of a single heated vertical plate. It is interesting to note that in the range $7 < Gr\,Pr < 100$, where the flow remains developing up to the tube exit, the simplified model still coincides with the numerical analysis. It should be mentioned that the *Nu* values for $\xi = 1.4$ and 1.8 of the model are practically the same.

EXPERIMENTAL APPARATUS AND PROCEDURE

Apparatus

The experimental apparatus A and B and the fiber velocity–deflection calibration setup are shown in Figs. 5(a)–(c), respectively. Apparatus A was utilized to examine the applicability of the simplified theory to a case of fully heated isothermal tube in a non-stratified ambient. In addition, the effects of the pressure loss coefficients ξ, ζ_0 and ζ_L and the dependence of fluid properties on temperature upon the average mass velocity are also demonstrated through apparatus A. Apparatus B was utilized to examine the applicability of the theory to cases of partly heated and partly cooled or partly adiabatic tube in stratified and non-stratified ambients.

The basic element of the apparatus was a copper tube of 10.5 mm i.d., or a polycarbonate tube of 11.1 mm i.d., with lengths of 375, 614 and 1120 mm for apparatus A and 1120×2 mm for apparatus B. The test tube was concentrically encased in a 50 mm diameter PVC tube, which was covered with 10 mm thick polyurethane insulation. The temperature of the test tube was maintained at different isothermal wall conditions by circulating water from a bath through the annular space between the copper and PVC tubes.

The wall temperature of the test tube was measured by five 50 μm c–c (copper–constantan) thermocouples, the hot junctions of which were bonded to the surface of the wall at the middle of the tube length and at distances of 5 and 50 mm from the tube ends. The ambient temperature was monitored by five 50 μm c–c thermocouples distributed along a vertical line that

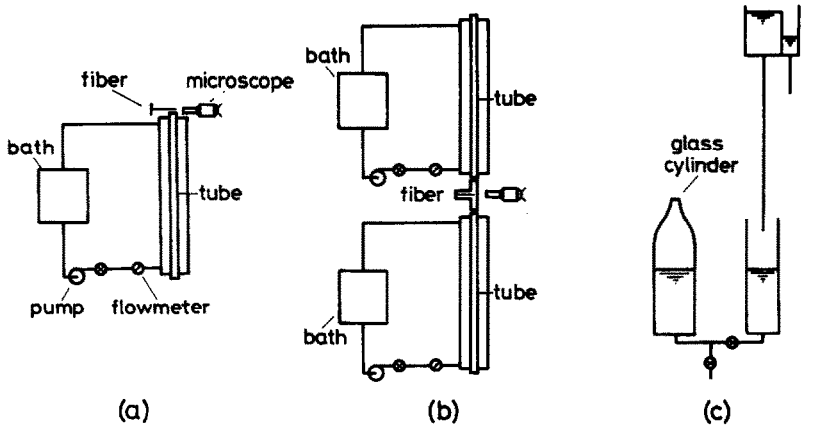

FIG. 5. Experimental apparatus and calibration setup: (a) apparatus A—single heated tube; (b) apparatus B—heated and cooled tube combination; (c) fiber deflection–velocity calibration setup.

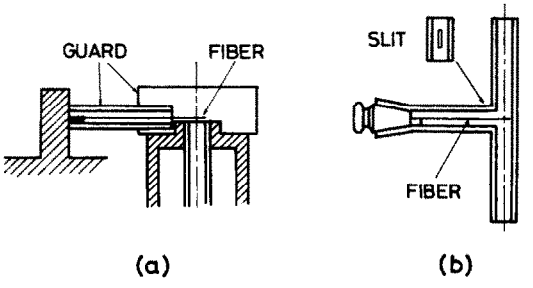

FIG. 6. Quartz fiber supports: (a) for apparatus A; (b) for apparatus B.

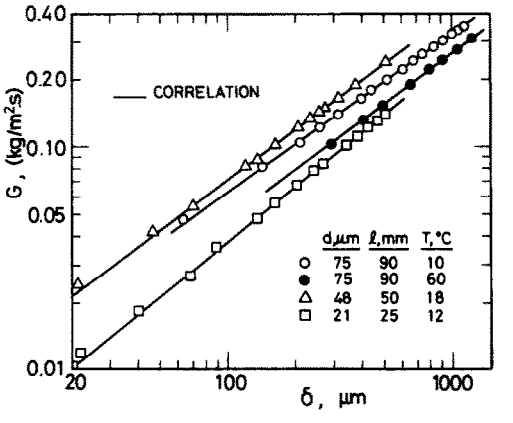

FIG. 7. Relation between average mass velocity G and quartz fiber deflection δ.

was displaced laterally from the tube axis by about 50 cm. The lowest hot junction was level with the lower end of the test tube and the uppermost one was level with the upper end of the test tube, while the others were equally spaced between them.

The tube's center-line temperature distribution for apparatus B was measured by a traversing 50 μm c–c thermocouple. The thermocouple was carried by a fine thread along the tube axis which was supported by two grooved rollers located outside the tube.

Apparatus A was placed in a large room, while apparatus B was placed inside a vinyl-made enclosure 4 m high with a floor area of 2×2 m. A steady temperature stratification was maintained inside the enclosure by a 600 W (max.) heater placed near to and facing one of its walls and by a 1 kW (max.) heater placed near to and facing its roof. The degree of stratification was controlled by the electric input to the heaters. The air movement in the core of the enclosure was found to be negligibly small.

Velocity measurement method

The velocity was measured by a quartz fiber anemometer. This method was applied by Schmidt and Beckmann [36], Tritton [37] and Currie and Newman [11] to determine the velocity distribution of natural convection flows. Unlike in past applications, the method is presently applied to measure directly the average mass velocity inside a tube.

Figures 6(a) and (b) schematically show the manner of using the instrument in the present study. One end of the fused quartz fiber was bonded to the rigid support while the other end was exposed transversely to the flow stream and deflected by drag force. A telemicroscope with a calibrated eyepiece was used to measure the deflection. For apparatus A the fiber was situated 1 mm above the tube exit while for apparatus B it was encased in a T-glass tube. The fiber was calibrated by the setup shown in Fig. 5(c). The reduced end of the glass cylinder was connected to the lower end of the test tube, and water was introduced at a constant flow rate into the glass cylinder in order to push air through the test tube. The average mass velocity G inside the test tube was obtained from the volume flow rate of the water.

Sample calibration results are shown in Fig. 7. The deviation of the measured points from the correlation curve is attributed to the ability of the calibration setup to produce constant velocity and presence of extraneous air currents and mechanical vibrations. The maximum deviation is smaller than 0.0035 kg $m^{-2} s^{-1}$.

The correlation curve depends on fluid temperature as ρ and μ of the fluid depend on temperature. This influence was clarified by calibrating a fiber of $d = 75$

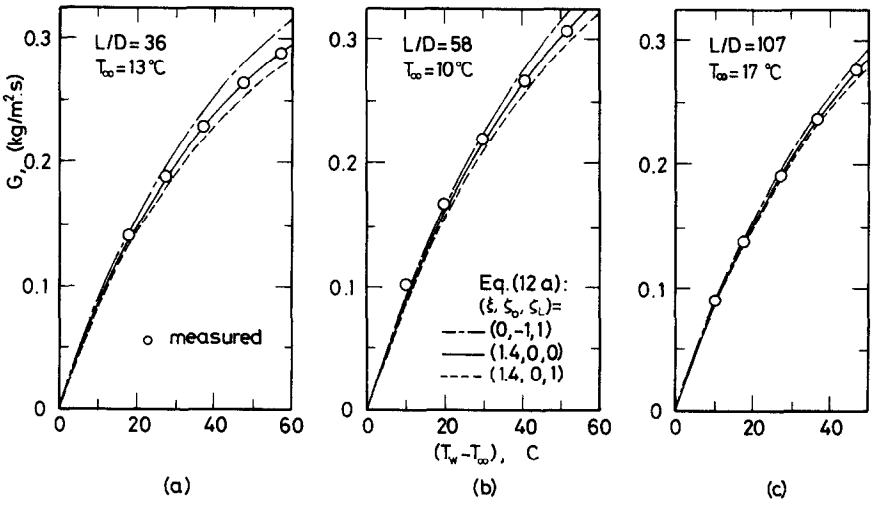

FIG. 8. Average mass velocity inside the isothermally heated vertical tube of apparatus A: (a) $L = 375$ mm; (b) $L = 614$ mm; (c) $L = 1120$ mm.

μm and $l = 90$ mm at 10 and 60°C. The results, which are marked respectively by symbols ○ and ● for temperatures 10 and 60°C in the figure, indicate that the 60°C curve shifts to the right by about 35% at $G = 0.3$ kg m^{-2} s^{-1} and by about 45% at $G = 0.1$ kg m^{-2} s^{-1}. Thus, for experimental apparatus A, the calibrations were made at two temperature levels (at a maximum heating temperature of the test tube and at room temperature) and the magnitudes of the temperature influence for other temperature levels were linearly interpolated from the two known calibration curves. The high temperature calibration was performed with the test tube section being isothermally heated. For experimental apparatus B, the calibration was made at room temperature only, because the fluid temperature within the T-glass section was always nearly equal to room temperature in the experiments. It should be mentioned that for the present experiment range (indicated in Fig. 2) the flow past the fiber is hydrodynamically and thermally developed. The uncertainty associated with the difference in velocity profile during calibration and application is negligible as long as the measurement is confined to this range.

EXPERIMENTAL RESULTS AND COMPARISON WITH THE SIMPLIFIED THEORY

Experiments for apparatus A

Figures 8(a)–(c) show the average mass velocity results for apparatus A with $L/D = 36$, 58 and 107, respectively. The measured values correspond to experimental conditions in the range $1 \leqslant Gr \leqslant 10$. In each figure the values predicted by the present theory using the following combinations of pressure loss coefficients $(\xi, \zeta_0, \zeta_L) = (1.4, 0, 1)$, $(1.4, 0, 0)$ and $(0, -1, 1)$ are represented by dashed, solid and chain lines, respectively. Computations using Kays' ζ values $(\xi, \zeta_0, \zeta_L) = (1.4, 1, 0.4)$ were also made and the results are very close to the dashed lines, and therefore are not plotted in the figure. These results are also very near to those of computations using (1.4, 1, 0). The solid lines agree well with the measured values. It should be remembered that the value of ξ is fixed at 1.4 prior to the selection of ζ_0 and ζ_L. Further, if the value $\xi = 1.4$ is used together with the tube-end conditions of the two-dimensional numerical analysis $\zeta_0 = -1$ and $\zeta_L = 1$ (or $p_0^* = 0$ and $p_L^* = 0$) the results are almost equal to the solid lines in the figure. This means that if $(p_0^* - p_L^*)$ is the same, practically the same value of G is obtained. The case $(\xi, \zeta_0, \zeta_L) = (0, -1, 1)$ corresponds to the simple Graetz problem. The effects of ξ and ζ on G decrease as L/D increases. Finally, at the lowest measured point in Fig. 8(c), which corresponds to $Gr = 1$, all lines merge and we may adopt this point as the criteria for long tubes. Thus, for a long tube $(Gr < 1)$ $\xi = 0$ and $\zeta = 0$ are appropriate.

Figure 9 shows the relationship between G and

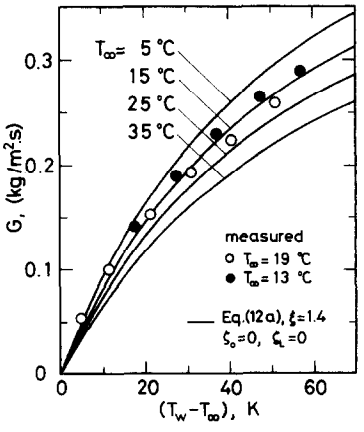

FIG. 9. Average mass velocity inside the isothermally heated vertical tube ($D = 10.5$ mm, $L = 375$ mm) of apparatus A for different ambient temperature levels.

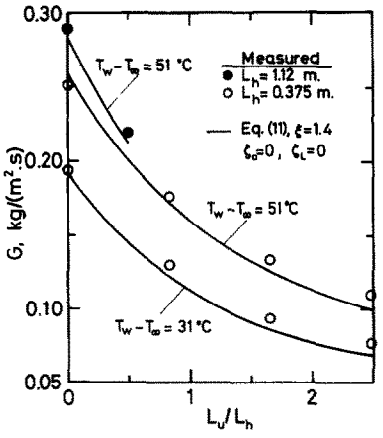

FIG. 10. Average mass velocity inside the isothermally heated vertical tube of apparatus A when an unheated tube of the same diameter is connected to its lower end.

$(T_w - T_\infty)$ with T_∞ as a parameter for $L/D = 36$, where different T_∞ levels mean different air temperature levels inside the tube for the same value of $(T_w - T_\infty)$. It is seen that the effect of the temperature dependence of physical properties of the fluid on the mass velocity is remarkable, and the trend and magnitude of the measured values agree with theory, though the temperature range of the measurements presented is narrow.

Figure 10 shows the mass velocity for the case where an unheated tube of the same diameter as the test tube is attached to the lower end of the test tube of apparatus A. The ratio of the unheated to the heated length L_u/L_h is taken as the abscissa. The good agreement between theory and experiment shows the applicability of the present theory to the situation on hand. Close observation, however, reveals that the measured values are slightly higher than the predicted ones. This discrepancy is attributed to the heat conducted from the heated test tube to the unheated tube.

Experiments for apparatus B

Table 1 shows the experimental conditions for apparatus B.

Figures 11(a) and (b) show examples of measured data on center-line fluid temperature (○), tube wall temperature (●) and ambient temperature (◇). Figure 11(a) corresponds to Case 3, where the upper tube is heated and the lower tube is cooled, while Fig. 11(b) corresponds to Case 4, where the upper tube is cooled and the lower tube is heated. A corresponding sketch of the tube is shown in the right-hand margin of the figure.

For large L/D, as in the case of apparatus B, the fluid temperature inside the tube is almost the same as the tube wall temperature except near the upper and lower ends of each tube. Therefore, the average fluid temperature T can be approximated by the measured values of T_w and T_∞ as follows:

$$\begin{aligned} 0 < x < L_1; &\quad T = T_{wD} \\ L_1 < x < L_2; &\quad T = T_{\infty, L/2} \\ L_2 < x < L_3; &\quad T = T_{wU} \end{aligned} \tag{14}$$

where $L_1 = 1.12$ m, $L_2 = 1.26$ m and $L_3 = 2.38$ m shown in the figure are scarcely affected by the experimental conditions. The ambient temperature T_∞ in Fig. 11(a) is linear and that in Fig. 11(b) is approximated by a bent line.

As L/D is large, the effects of the inertia and pressure terms on the mass velocity are small, and it could be possible to predict G by using equations (13) and (14). For a linear ambient temperature expressed as

$$T_\infty = T_{\infty 0} + \frac{T_{\infty L} - T_{\infty 0}}{L} x = T_{\infty 0} + k_1 x \tag{15}$$

and values of density ρ and viscosity μ of air approximated by

$$\rho = 3.483 \times 10^{-3} \frac{p}{T} = \frac{352.8}{T} = \frac{k_2}{T} \ [\mathrm{kg\,m^{-3}}] \tag{16}$$

$$\begin{aligned} \mu &= 4.39 \times 10^{-6} + 4.70 \times 10^{-8} T \\ &= k_3 + k_4 T \ [\mathrm{Pa\,s}] \end{aligned} \tag{17}$$

in the range $270 < T < 370$ K, the terms for fluid resistance F and buoyancy B are expressed by substituting equations (14)–(17) into equations (8) and (9) as

$$\begin{aligned} F = \frac{32}{k_2 D^2} \{ &(k_3 T_{wD} + k_4 T_{wD}^2) L_1 \\ &+ (k_3 T_{\infty, L/2} + k_4 T_{\infty, L/2}^2)(L_2 - L_1) \\ &+ (k_3 T_{wU} + k_4 T_{wU}^2)(L_3 - L_2) \} \end{aligned} \tag{18}$$

and

Table 1. Experimental conditions for apparatus B

Case No.	Upper tube	Lower tube	Ambient	Tube material
1	heated	at T_∞	nonstratified	copper
2	heated	0°C	nonstratified	copper
3	heated	0°C	stratified	copper
4	0°C	heated	stratified	copper
5	heated	0°C	stratified	polycarbonate

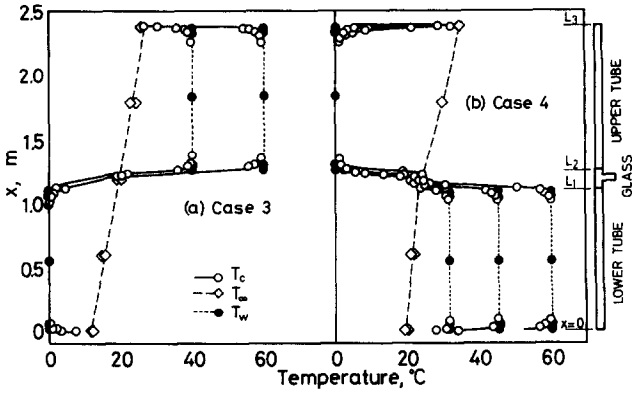

FIG. 11. Measured center-line, tube wall and ambient temperatures for apparatus B: (a) upper tube is heated while lower tube is cooled; (b) upper tube is cooled while lower tube is heated.

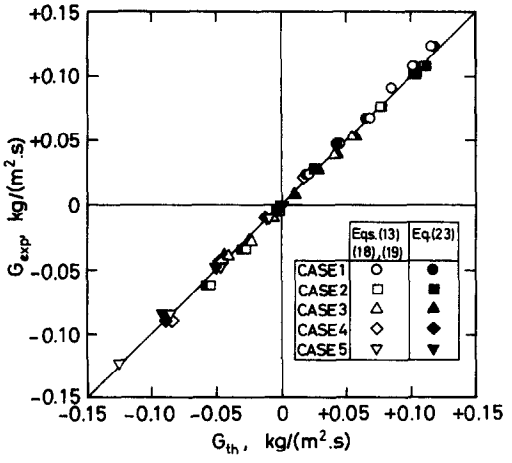

FIG. 12. Comparison between the measured and the predicted average mass velocities for apparatus B.

$$B = k_2 g\left\{\frac{1}{k_1}\ln\frac{(T_{\infty 0}+k_1L_1)(T_{\infty 0}+k_1L_3)}{T_{\infty 0}(T_{\infty 0}+k_1L_2)} - \left(\frac{L_1}{T_{wD}}+\frac{L_3-L_2}{T_{wU}}\right)\right\}. \quad (19)$$

In Fig. 12 the predicted values G_{th} obtained by equations (13), (18) and (19) compare well with the measured values G_{exp}. For the non-linear ambient fluid temperature cases, equation (15) is sectionally applied to vertical distance segments. In the figure, positive G means upward flow, while negative G means downward flow.

When $(L_2-L_1) \ll L$ is assumed, that is $L_1 = L_3-L_2 = L/2$, equations (18) and (19) are reduced to

$$F = \frac{16L}{k_2D^2}\{k_3(T_{wD}+T_{wU})+k_4(T_{wD}^2+T_{wU}^2)\} \quad (20)$$

and

$$B = gk_2L\left\{\frac{\ln(T_{\infty L}/T_{\infty 0})}{(T_{\infty L}-T_{\infty 0})} - \frac{1}{2}\left(\frac{1}{T_{wD}}+\frac{1}{T_{wU}}\right)\right\}. \quad (21)$$

In equation (21), a representative temperature $T_{\infty e}$ for the ambient temperature can be defined in the case of a linear stratification as

$$\frac{1}{T_{\infty e}} = \frac{\ln(T_{\infty L}/T_{\infty 0})}{T_{\infty L}-T_{\infty 0}} \doteqdot \frac{2}{T_{\infty 0}+T_{\infty L}}. \quad (22)$$

For the case where the ambient temperature distribution is not linear, trial calculations reveal that $T_{\infty e}$ can be approximated by the value of T_∞ averaged over the tube height. Therefore, the mass velocity can be predicted simply by

$$G_{th} = \frac{gk_2^2D^2}{16} \times\left\{\frac{\frac{1}{T_{\infty e}}-\frac{1}{2}\left(\frac{1}{T_{wD}}+\frac{1}{T_{wU}}\right)}{k_3(T_{wD}+T_{wU})+k_4(T_{wD}^2+T_{wU}^2)}\right\}. \quad (23)$$

The values predicted by equation (23) also agree fairly well with the experimental values G_{exp} as shown by the symbols ●, ■, ▲, ◆ and ▼ in Fig. 12.

The condition that fluid flow does not take place due to a balance between positive and negative buoyancy forces is expressed as

$$\frac{1}{(T_{\infty e})_{cri}} = \frac{1}{2}\left(\frac{1}{T_{wD}}+\frac{1}{T_{wU}}\right). \quad (24)$$

This relation is verified by plotting G_{exp} against $[1/T_{\infty e}-(1/T_{wD}+1/T_{wU})/2]$ in Fig. 13. It should be remembered that $(T_{\infty e})_{cri}$ is not the arithmetic mean of T_{wD} and T_{wU}, but $(T_{\infty e})_{cri}$ is related to T_w in the following manner $[T_{wU}-(T_{\infty e})_{cri}] > [(T_{\infty e})_{cri}-T_{wD}]$.

CONCLUDING REMARKS

Free convection inside an isothermally heated or cooled vertical tube placed in a large space was experimentally and theoretically studied.

(1) There is proposed a simplified one-dimensional theory which is based on the Graetz solution for

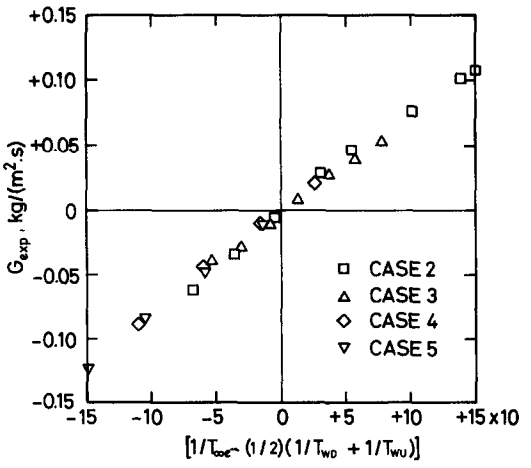

FIG. 13. Measured average mass velocity G_{exp} vs $[1/T_{\infty e}-(1/T_{wD}+1/T_{wU})/2]$ for apparatus B.

forced convection heat transfer and which considers the pressure losses in the flow developing region and at the tube inlet and exit.

(2) By comparing the proposed theory with the two-dimensional numerical analysis, the range of applicability of the theory is confirmed to be $Gr\,Pr < 100$. This range includes flows which remain developing up to the tube exit. The agreement between the theory and the numerical analysis in terms of volumetric flow rate and dimensionless heat transfer coefficient Nu has been confirmed.

(3) The average mass velocity of air inside a tube has been effectively measured by means of the deflection of a fused quartz fiber set in cross flow.

(4) The agreement between theory and experiment has been confirmed for the cases where the tube is fully heated, and partly heated and partly cooled or partly adiabatic.

(5) For a short tube ($Gr > 1$), the effect of the pressure loss due to velocity development in the entrance region on the mass velocity is remarkable while that of the additional pressure losses ζ_0 and ζ_L are small. For a long tube ($Gr < 1$), the effects of these pressure losses are negligible and the mass velocity is simply determined by the ratio of the total buoyancy to the total flow resistance.

(6) In the prediction of mass velocity for a long tube placed in a thermally stratified ambient fluid, the ambient temperature averaged over the tube height can be taken as a representative temperature of the ambient; and this representative value can also be used for the determination of the no-flow condition when the positive and negative buoyancy forces are in balance as represented by equation (24).

(7) Demonstrations on the effects of $(T_w - T_\infty)$, L/D and temperature dependence of fluid properties upon mass velocity are made using the present experimental apparatus and conditions.

Acknowledgement—This work was accomplished under the grant in aid for scientific research of the Ministry of Education Science and Culture of Japan (Grant No. 61040026).

REFERENCES

1. F. Grashof, Theorie der zugerzeugung durch schortsteine, *VDI Abhandlungen* **10,** 431–462 and 497–514 (1866).
2. L. G. Carpenter and H. C. Wassell, The loss of heat by natural convection from parallel vertical plates in air, *Proc. Instn Mech. Engrs* **128,** 439–457 (1934).
3. W. Elenbaas, Heat dissipation of parallel plates by free convection, *Physica* **9,** 1–28 (1942).
4. W. Elenbaas, The dissipation of heat by free convection from the inner surface of vertical tubes of different shapes of cross-section, *Physica* **9,** 865–874 (1942).
5. A. Kobayashi and Y. Fujimoto, Study of heat dissipation by natural convection between parallel vertical plates, *Trans. J.S.M.E.* **20,** 233–237 (1954), in Japanese.
6. J. R. Bodoia and F. J. Osterle, The development of free convection between heated vertical plates, *ASME J. Heat Transfer* **84,** 40–44 (1962).
7. T. Aihara, Heat transfer due to natural convection from parallel vertical plates, *Trans. J.S.M.E.* **29,** 903–909 (1963), in Japanese.
8. S. Ostrach, Laminar flows with body forces. In *Theory of Laminar Flows* (Edited by F. K. Moore), Section F. Princeton University Press, Princeton, New Jersey (1964).
9. T. S. Lauber and A. U. Welch, Natural convection heat transfer between vertical flat plates with uniform heat flux, *Proc. of the Third Int. Heat Transfer Conference*, Vol. II, pp. 126–131 (1966).
10. J. L. Novotny, Laminar free convection between finite vertical parallel plates. In *Progress in Heat and Mass Transfer* (Edited by T. F. Irvine, Jr.), Vol. 2, pp. 13–22. Pergamon Press, New York (1969).
11. I. G. Currie and W. A. Newman, Natural convection between isothermal vertical surfaces, *Proc. of the Fourth Int. Heat Transfer Conference*, Vol. IV, NC2.7 (1970).
12. J. R. Dyer, The development of laminar natural convection flow in a vertical duct of circular cross-section that has a flow restriction at the bottom, *Proc. of the Fourth Int. Heat Transfer Conference*, Vol. IV, NC2.8 (1970).
13. M. Kageyama and R. Izumi, Natural convection in a vertical circular tube, *Bull. J.S.M.E.* **13,** 382–394 (1970).
14. L. P. Davis and J. J. Perona, Development of free convection flow of a gas in a heated vertical open tube, *Int. J. Heat Mass Transfer* **14,** 889–903 (1971).
15. O. Miyatake and T. Fujii, Free convection heat transfer between vertical parallel plates—one plate isothermally heated and the other thermally insulated, *Heat Transfer—Jap. Res.* **1,** 30–38 (1972).
16. O. Miyatake, T. Fujii, M. Fujii and H. Tanaka, Natural convective heat transfer between vertical parallel plates—one plate with a uniform heat flux and the other thermally insulated, *Heat Transfer—Jap. Res.* **2,** 25–33 (1973).
17. W. Aung, Fully developed laminar free convection between vertical plates heated asymmetrically, *Int. J. Heat Mass Transfer* **15,** 1577–1580 (1972).
18. W. Aung, L. S. Fletcher and V. Sernas, Developing laminar free convection between vertical flat plates with asymmetric heating, *Int. J. Heat Mass Transfer* **15,** 2293–2308 (1972).
19. O. Miyatake and T. Fujii, Natural convective heat transfer between vertical parallel plates with unequal uniform temperatures, *Heat Transfer—Jap. Res.* **2,** 79–88 (1973).
20. T. Aihara, Effects of inlet boundary-conditions on numerical solutions of free convection between vertical parallel plates, *Rep. Inst. High Speed Mech. Tohoku Univ.* **28,** 1–27 (1973).
21. J. Quintiere and W. K. Mueller, An analysis of laminar free and forced convection between finite vertical parallel plates, *ASME J. Heat Transfer* **95,** 53–59 (1973).

22. O. Miyatake and T. Fujii, Natural convective heat transfer between vertical parallel plates with unequal heat fluxes, *Heat Transfer—Jap. Res.* **3**, 29–33 (1974).
23. J. R. Dyer, The development of laminar natural-convective flow in a vertical uniform heat flux duct, *Int. J. Heat Mass Transfer* **18**, 1455–1465 (1975).
24. J. R. Dyer, Natural-convective flow through a vertical duct with a restricted entry, *Int. J. Heat Mass Transfer* **21**, 1341–1354 (1978).
25. H. Akbari and T. R. Borgers, Free convective laminar flow within the Trombe wall channel, *Sol. Energy* **22**, 165–174 (1979).
26. E. M. Sparrow and P. A. Bahrami, Experiments on natural convection from vertical parallel plates with either open or closed edges, *ASME J. Heat Transfer* **102**, 221–227 (1980).
27. H. Nakamura, Y. Asako and T. Naitou, Heat transfer by free convection between parallel flat plates, *Numer. Heat Transfer* **5**, 95–106 (1982).
28. A. Bar-Cohen and W. M. Rohsenow, Thermally optimum spacing of vertical, natural convection cooled, parallel plates, *ASME J. Heat Transfer* **106**, 116–123 (1984).
29. E. M. Sparrow, G. M. Chrysler and L. F. Azevedo, Observed flow reversals and measured-predicted Nusselt numbers for natural convection in a one-sided heated vertical channel, *ASME J. Heat Transfer* **106**, 325–332 (1984).
30. T. Yamasaki and T. F. Irvine, Jr., Laminar free convection in a vertical tube with temperature-dependent viscosity, *Int. J. Heat Mass Transfer* **27**, 1613–1621 (1984).
31. E. M. Sparrow and L. F. Azevedo, Vertical-channel natural convection spanning between the fully-developed limit and the single-plate boundary-layer limit, *Int. J. Heat Mass Transfer* **28**, 1847–1857 (1985).
32. T. Aihara, S. Maruyama and J. S. Choi, Laminar free convection with variable fluid properties in vertical ducts of different cross-sectional shapes, *Proc. of the Eighth Int. Heat Transfer Conference*, Vol. 4, pp. 1581–1586 (1986).
33. F. W. Schmidt and B. Zeldin, Laminar flows in inlet sections of tubes and ducts, *A.I.Ch.E. Jl* **15**, 612–614 (1969).
34. R. Y. Chen, Flow in the entrance region at low Reynolds numbers, *Trans. ASME J. Fluid Engng* **95**, 153–158 (1973).
35. W. M. Kays, Loss coefficients for abrupt changes in flow cross section with low Reynolds number flow in single and multiple-tube systems, *Trans. ASME* **72**, 1067–1074 (1950).
36. E. Schmidt und W. Beckmann, Das Temperatur- und Geshwindigkeitsfeld vor einer Wärme abgebenden senkrechten Platte bei natürlicher Konvektion, *Tech. Mech. Thermo-Dynam.* **1**(10), 341–349 (1930).
37. D. Tritton, Turbulent free convection above a heated plate inclined at a small angle to the horizontal, *J. Fluid Mech.* **16**, 282–312 (1963).
38. G. M. Brown, Heat or mass transfer in a fluid in laminar flow in a circular or flat conduit, *A.I.Ch.E. Jl* **6**, 179–183 (1960).

APPENDIX: K_n VALUES IN EQUATION (10)

The values of K_n in equation (10) are determined by the following equation:

$$K_n = \frac{-4\int_0^1 R_n r^* \, dr^*}{\lambda_n \left(\frac{\partial R_n}{\partial \lambda_n}\right)_{r^*=1}} \tag{A1}$$

where λ_n and R_n are the nth eigenvalue and the nth eigenfunction of the Graetz solution, respectively, and r^* is the dimensionless radial coordinate of the tube. The first six values of K_n were evaluated by Simpson's rule for integration employing 20 radial nodes and by using the values of λ_n, R_n and $(\partial R_n/\partial \lambda_n)_{r^*=1}$ given by Brown [38]. The results are shown in Table A1.

Table A1. Values of λ_n given by Brown [38] and K_n determined by equation (A1) for equation (10)

n	λ_n	K_n
1	2.70436 44199	0.58112 21007
2	6.67903 14493	0.13376 65498
3	10.67337 95381	0.06189 20492
4	14.67107 84627	0.03659 59673
5	18.66987 18645	0.02459 18544
6	22.66914 33588	0.01779 87035

CONVECTION NATURELLE LAMINAIRE DANS UN TUBE VERTICAL

Résumé—On considère l'écoulement de convection naturelle laminaire dans un tube vertical complètement chauffé ou partiellement chauffé et partiellement refroidi, placé dans un large espace. Une théorie basée sur un modèle unidimensionnel qui utilise la solution de Graetz pour la convection forcée dans un tube et qui considère les pertes de pression à l'entrée et à la sortie et dans la région de développement, est proposée pour le domaine $Gr\,Pr < 100$. Pour le tube entièrement chauffé, la théorie est comparée avec une analyse numérique bidimensionnelle et des mesures récentes faites avec un anémomètre à fibre de quartz. Leur accord est bon quand des valeurs convenables de coefficient de perte de pression sont utilisées dans la théorie. Pour le tube partiellement chauffé et partiellement refroidi ou partiellement adiabatique dans des ambiances thermiquement stratifiées et non stratifiées, l'accord entre théorie et expériences est aussi satisfaisante. On clarifie les effets sur le débit-masse moyen dans le tube de la différence de température tube-ambiance, de la température représentative de l'ambiance stratifiée, du rapport longueur/diamètre du tube et de la variation des propriétés du fluide vis-à-vis de la température.

LAMINARE NATÜRLICHE KONVEKTION IN EINEM VERTIKALEN ROHR

Zusammenfassung—Diese Arbeit behandelt die laminare natürliche Konvektion in einem völlig beheizten oder teilweise beheizten und teilweise gekühlten vertikalen Rohr, das sich in einem großen Raum befindet. Für den Bereich $Gr\,Pr < 100$ wird eine Theorie vorgeschlagen, welche auf einem eindimensionalen Modell aufbaut, die Graetz-Lösung für erzwungene Konvektion in einem Rohr benutzt und die Druckverluste am Rohreingang und -ausgang und in der hydrodynamischen Einlaufstrecke berücksichtigt. Für das völlig beheizte Rohr wird die Theorie mit einer zweidimensionalen numerischen Berechnung und mit Messungen mit einem Quarzfaseranemometer verglichen. Die Übereinstimmung ist gut, wenn geeignete Druckverlustbeiwerte in der Theorie verwendet werden. Für das teilweise beheizte und teilweise gekühlte oder teilweise adiabatische Rohr in thermisch geschichteter oder ungeschichteter Umgebung ist die Übereinstimmung zwischen Theorie und Experiment ebenfalls gut. Außerdem wird auf die Einflüsse der Temperaturdifferenz zwischen Rohr und Umgebung, der mittleren Temperatur der geschichteteten Umgebung, des Verhältnisses Länge zu Durchmesser des Rohres und der Temperaturabhängigkeit der Stoffwerte auf die mittlere Massenstromdichte im Rohr eingegangen.

СКОРОСТЬ ЛАМИНАРНОГО СВОБОДНОКОНВЕКТИВНОГО ПОТОКА В ВЕРТИКАЛЬНОЙ ТРУБЕ

Аннотация—Рассматривается скорость ламинарного свободноконвективного потока внутри полностью или частично нагретой и частично охлажденной вертикальной турбы, находящейся в неограниченной среде. Теория, основанная на одномерной модели, использующей решение Грэтца для вынужденной конвекции в трубе и учитывающей потери давления как на входе, так и на выходе из трубы, а также в области гидродинамической стабилизации, предложена для $Gr\,Pr < 100$. Для случая полностью нагретой турбы теория сравнивается с результатами двумерного численного моделирования и измерениями, проведенными с помощью анемометра с кварцевой нитью. Найдено их хорошее соответствие при использовании в теории соответствующих коэффициентов потери давления. В случае частично нагретой и частично охлажденной или частично адиабатической турбы, окруженной нестратифицированной средой или сердой с тепловой стратификацией, соответствие между теорией и экспериментом тоже хорошее. Выясняется влияние на средний массовый расход внутри трубы разности температур между трубой и окружающей средой, характерной температуры стратифицированной среды, отношения длины трубы к ее диаметру и температурной зависимости свойств жидкости.